

A Highly Noise-Immune Capacitive Touch Sensing System Using an Adaptive Chopper Stabilization Method

Jae-Sung An, *Student Member, IEEE*, Sung-Jin Jung, *Student Member, IEEE*, Seong-Kwan Hong, *Member, IEEE*, and Oh-Kyong Kwon, *Member, IEEE*

Abstract—This paper proposes a capacitive touch sensing system (CTSS) using an adaptive chopper stabilization (ACS) method to achieve high noise immunity. The proposed ACS method quickly detects and adaptively filters out external noises, thereby achieving high noise immunity in the proposed CTSS. To verify the proposed ACS method, a readout integrated circuit (ROIC) was fabricated using a 0.35 μm CMOS process technology with 18 V high-voltage devices and was measured using a 46-inch capacitive touch sensor (CTS). When no external noises are induced into the CTS, the measured signal-to-noise ratio (SNR) of the ROIC is 45.8 dB at a reporting rate of 120 Hz. When external noises are induced into the CTS, the measured SNR of the ROIC using the ACS method is 44.5 dB, which is improved by 22.0 dB compared to the SNR achieved without using the ACS method. Therefore, the proposed ACS method effectively eliminates external noises induced into the CTS of the CTSS.

Index Terms— Capacitive touch sensor, touch sensing system, capacitive touch sensor, band-pass filter, chopper-stabilization, noise immunity.

I. INTRODUCTION

TOUCH sensing systems are widely used in various applications such as smart watches, smart phones, tablet PCs, TVs, kiosks, and interactive white boards [1]-[6]. Among touch sensing systems, the capacitive touch sensing system (CTSS) is increasingly used because of its multi-touch capability, high sensitivity, and durability [4]-[6].

In the CTSS, external noises such as display and conduction noises are continuously induced into the capacitive touch sensor (CTS), resulting in decreasing the signal-to-noise ratio (SNR) of the CTSS [7]-[9]. Thus, several sensing methods, such as integration method [9]-[10], differential sensing method [12]-[13], and chopper stabilization method [13], have been researched in attempts to eliminate these noises and enhance the SNR.

Integration and differential sensing methods reduce external noises using the difference between the charge signals that are sensed from two adjacent receiver (RX) electrodes of the CTS. However, the electrical characteristics of RX electrodes differ

J.-S. An, S.-J. Jung, S.-K. Hong, and O.-K. Kwon are with the Department of Electronic Engineering, Hanyang University, 222 Wangsimni-ro, Seongdong-gu, Seoul, 04763, Korea (phone: +82-2-2220-0359; fax: +82-2-2297-2232; e-mail: okwon@hanyang.ac.kr).

from one another due to process variations. Moreover, because the capacitance between the conductor and the RX electrode is not equal to that between the conductor and the adjacent RX electrode, the external noise cannot be effectively filtered out. The chopper stabilization method selectively filters out external noises and senses the charge signal at a single RX electrode to achieve high SNR. However, when the frequency of the external noise is near that of the excitation signal, the external noise is not reduced as significantly. To overcome the above issues, a noise detection algorithm [14] that operates by selecting the frequency of the excitation signal has been investigated, but this requires additional noise detection time and circuitry.

In this paper, we propose an adaptive chopper stabilization (ACS) method to achieve high noise immunity. The adaptive chopping controller (ACC) is implemented in the readout IC (ROIC) to quickly detect external noises and select an optimal set of frequencies. In addition, the chopper stabilization method with a synchronized band-pass filter (BPF) is employed in the readout circuit to filter out external noises using the above set of frequencies.

This paper is organized as follows. Section II describes the architecture and operating principle of the proposed ROIC. Section III explains how the proposed ACS method effectively detects and reduces external noises to enhance the SNR. Section IV describes the circuit implementation of the readout circuit in detail. The experimental results are analyzed and compared with previous works in Section V. Finally, conclusions are given in Section VI.

II. ARCHITECTURE OF THE PROPOSED ROIC

Fig. 1(a) shows the block diagram of the proposed CTSS which includes ROICs, a CTS, and touch data processor (TDP). The proposed ROIC consists of 44-channel readout circuits, 44-channel excitation circuits, an ACC, and a serial peripheral interface (SPI). The 44-channel excitation circuits sequentially send excitation signals to the transmitter (TX) electrodes ($\text{TX}[1:M]$) of the CTS. The excitation signals are converted to charge signals (V_{CS}) through the mutual capacitance (C_M) of each sensor pixel. The 44-channel readout circuits receive the V_{CS} from all RX electrodes, comprising $\text{RX}[1:N]$, filter out external noises such as conduction noise (V_{CN}) and display noise (V_{DN}), and then convert the V_{CS} to touch data. However, it

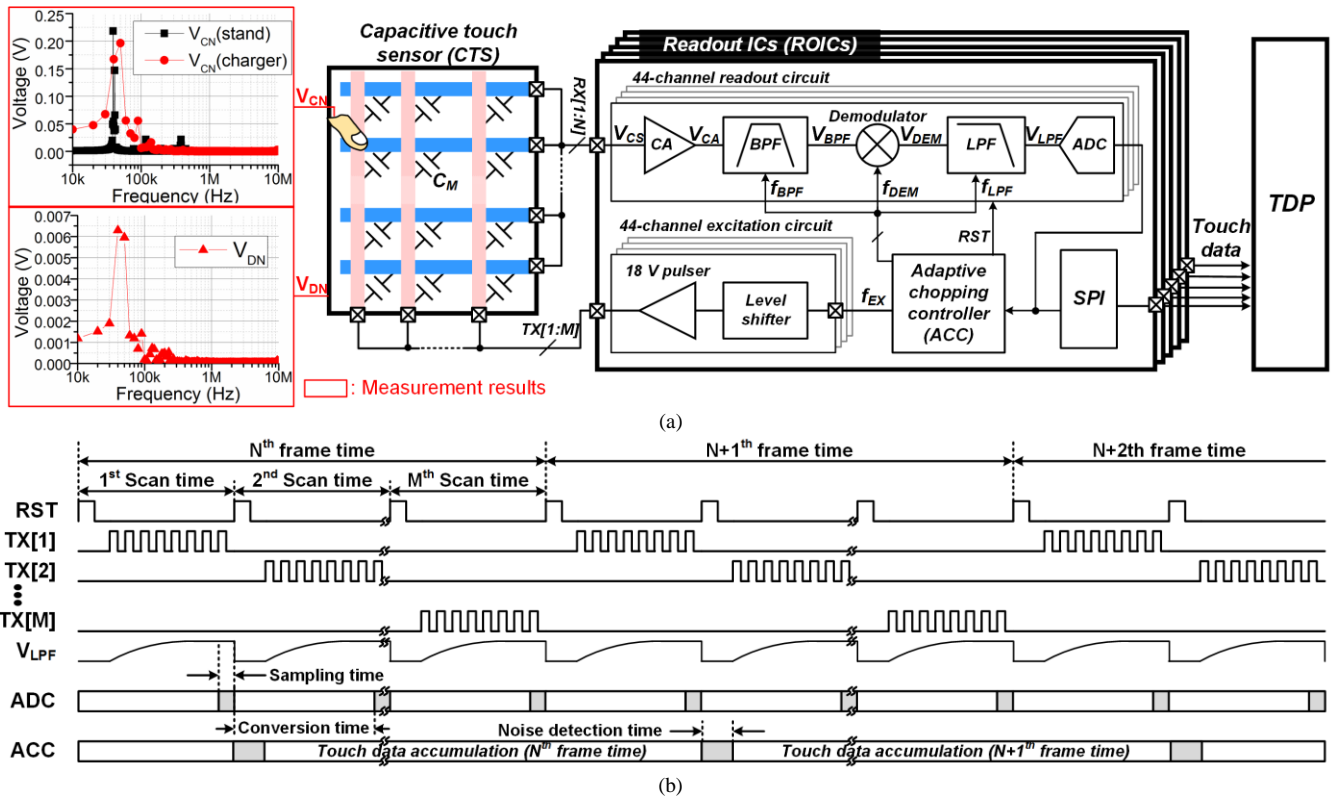


Fig. 1. (a) Block diagram of the proposed CTSS comprising an ROIC, CTS, and TDP, and (b) timing diagram of the proposed ROIC.

is difficult to filter out external noises whose frequencies are near that of the excitation signal. To solve this problem, the ACC is implemented in the proposed ROIC. The ACC utilizes touch data to detect the presence of external noises and to select an optimal set of frequencies which include the frequency of the excitation signal (f_{EX}) and its corresponding synchronously operating frequencies of the BPF, demodulator, and low-pass filter (LPF) (f_{BPF} , f_{DEM} , and f_{LPF} , respectively). The readout circuit adaptively filters out external noises using the above set of frequencies and transfers touch data to the TDP through the SPI.

Fig. 1(b) shows the timing diagram of the proposed ROIC. At each frame time, the excitation circuits receive f_{EX} from the ACC and sequentially send the excitation signals to each TX electrode of the CTS. When the scan time begins, the readout and excitation circuits are initialized by the reset signal (RST). After initialization, the excitation signal is applied to the TX electrode and converted to a V_{CS} through the C_M . Each readout circuit converts the V_{CS} to a voltage signal, namely as an output voltage of the LPF (V_{LPF}). The LPF filters out the high frequency signal of the output voltage of the demodulator (V_{DEM}); thus, the V_{LPF} , which is converted by the analog-to-digital converter (ADC), gradually increases and becomes saturated at the end of each scan time. To sample the saturated V_{LPF} in each scan time, the sampling time of the ADC is allocated at the end of each scan time and the conversion time of the ADC is assigned to extract the touch data before the next sampling time begins. To secure sufficient conversion time for converting the variation in V_{LPF} to high-resolution touch data, a single-slope ADC (SS-ADC) is implemented in each ROIC

[16]. After the first scan time of the next frame ends, the C_M of all sensor pixels are converted to touch data. Using these touch data, the ACC detects the presence of external noises and adaptively selects an optimal set of f_{EX} , f_{BPF} , f_{DEM} , and f_{LPF} to filter external noises out, without requiring any additional circuitry or noise detection time.

III. THE PROPOSED ADAPTIVE CHOPPER STABILIZATION (ACS) METHOD

A. Adaptive Chopping Controller (ACC) with Chopper Stabilization Method

Because external noises are continuously induced into the CTS [9] and the readout circuit is directly connected to the CTS, external noises heavily influence the touch data of all sensor pixels, decreasing the noise immunity of the CTSS. To enhance the noise immunity, an ACC is implemented in the ROIC that detects external noises and adaptively selects an optimal set of f_{EX} , f_{BPF} , f_{DEM} , and f_{LPF} to filter them out. In addition, because the influence of external noises on the ROIC gradually decreases as f_{EX} is moved farther from the frequency of external noises, a chopper stabilization method, which increases f_{EX} and filters out external noises, is employed to achieve high SNR of the ROIC [13]. However, as f_{EX} increases, two problems occur in the ROIC; the increase of power consumption and the attenuation of the amplitude of V_{CS} . To overcome the above issues, it is necessary to set f_{EX} as low as possible to reduce the power consumption of the ROIC while maintaining high SNR. To prevent the influence of external noise, including aliasing, f_{EX} should be no less than 10 times the greatest frequency of external noises. In addition, f_{EX} should be no higher than the bandwidth of the CTS to prevent the attenuation of the

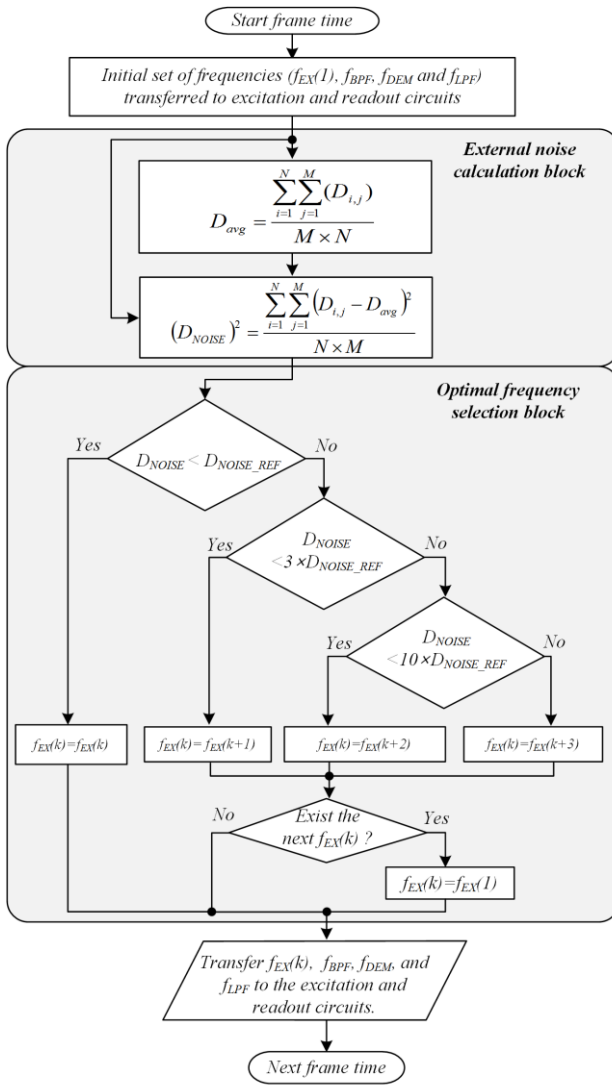


Fig. 2. Algorithm flowchart of the proposed ACS method in the ACC.

amplitude of V_{CS} ; such attenuation would occur because the CTS acts as a first-order low-pass filter at these frequencies. Taking into account the above considerations, the frequency spectra of f_{EX} should be selected between hundreds of kHz (because the external noises are spread over the range from tens of Hz to tens of kHz as shown in Fig. 1(a)) and a frequency of less than the bandwidth of the CTS. Among the selectable frequency sets, a set of the lowest frequencies is used in the readout circuit to obtain the touch data from the sensor pixels. Using the touch data, a pre-defined reference noise level (D_{NOISE_REF}) is determined to select an optimal set of frequencies according to the target SNR of the ROIC.

B. Algorithm Flowchart of the Proposed ACS Method

Fig. 2 shows an algorithm flowchart of the proposed ACS method implemented in the ACC, including external noise calculation and optimal frequency selection blocks. When the frame time begins, the ACC provides the initial set of frequencies ($f_{EX}(1)$, f_{BPF} , f_{DEM} , and f_{LPF}) to the excitation and readout circuits.

In the external noise calculation block, the average value of

touch data (D_{avg}) is calculated as

$$D_{avg} = \frac{\sum_{i=1}^N \sum_{j=1}^M (D_{i,j})}{N \times M}, \quad (1)$$

where $D_{i,j}$ is the touch data that is located at the intersection of the i -th RX and j -th TX electrodes. N and M are the numbers of RX and TX electrodes, respectively. Using $D_{i,j}$ and D_{avg} , the external noise level (D_{NOISE}) is calculated from the following equation,

$$(D_{NOISE})^2 = \frac{\sum_{i=1}^N \sum_{j=1}^M (D_{i,j} - D_{avg})^2}{N \times M}. \quad (2)$$

In the optimal frequency selection block, an optimal set of frequencies is quickly determined by comparing the calculated D_{NOISE} with three reference noise levels in sequence: D_{NOISE_REF} , $3 \times D_{NOISE_REF}$, and $10 \times D_{NOISE_REF}$, which respectively represent the SNRs of the ROIC at the 40, 30, and 20 dB thresholds. The SNR at the 40 dB threshold was chosen by determining the lowest f_{EX} to be at least 10 times greater than the frequency of external noises, as previously described in Section III.A, and the roll-off of the BPF is -40 dB/decade [16]. The SNRs of the 30 and 20 dB thresholds were determined to secure a sufficient f_{EX} shift margin from variation in mid-frequency of the BPF.

If D_{NOISE} is less than D_{NOISE_REF} , the initial set of frequencies $f_{EX}(n)$ is continuously used in the ROIC (Fig. 2). If D_{NOISE} is greater than D_{NOISE_REF} , the reference noise level is set to $3 \times D_{NOISE_REF}$ and compared with D_{NOISE} . Then, if D_{NOISE} is less than $3 \times D_{NOISE_REF}$, the SNR of the ROIC is considered to be between 30 and 40 dB, and $f_{EX}(n+1)$ is selected. If D_{NOISE} is greater than $3 \times D_{NOISE_REF}$, the SNR of the ROIC is considered to be less than 30 dB. Then the reference noise level is set to $10 \times D_{NOISE_REF}$ and compared with D_{NOISE} to determine whether the SNR of the ROIC is less than 20 dB. If D_{NOISE} is less than $10 \times D_{NOISE_REF}$, the SNR of the ROIC is considered to be between 20 and 30 dB, and $f_{EX}(n+2)$ is selected. If D_{NOISE} is greater than $10 \times D_{NOISE_REF}$, the SNR of the ROIC is considered to be less than 20 dB, and $f_{EX}(n+3)$ is selected. If the next f_{EX} no longer exists in the ACC, $f_{EX}(1)$ is selected. This process is iterated for every frame time until an optimal set of f_{EX} , f_{BPF} , f_{DEM} , and f_{LPF} is determined.

C. Operating Principle of the Readout Circuit

Fig. 3 illustrates the operation process of the chopper stabilization method using frequency spectra at each internal nodes of the readout circuit shown in Fig. 1(a). When the excitation signal with a selected f_{EX} is applied to the CTS, the C_M is converted and modulated to a V_{Cs} , which includes signals with f_{EX} and its harmonic frequencies (f_{EX_H}), and various noises such as 60 Hz interference and other external noises. Because the 60 Hz interference has a larger amplitude than the other external noises, it may saturate the output of the charge amplifier (V_{CA}). To prevent such saturation, the charge amplifier (CA) is designed as a high-pass filter, which attenuates the 60 Hz interference. Thus, because the CTS

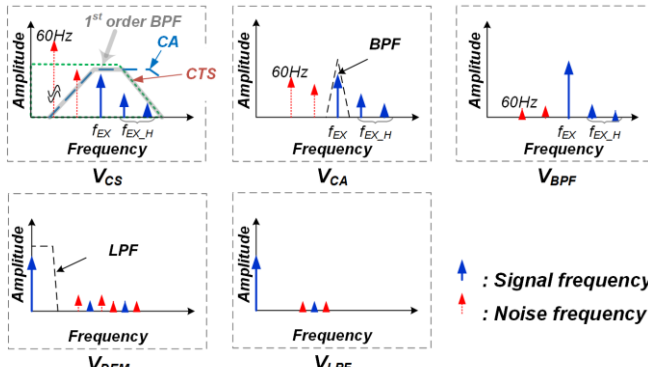


Fig. 3. Frequency spectra at internal nodes of the readout circuit.

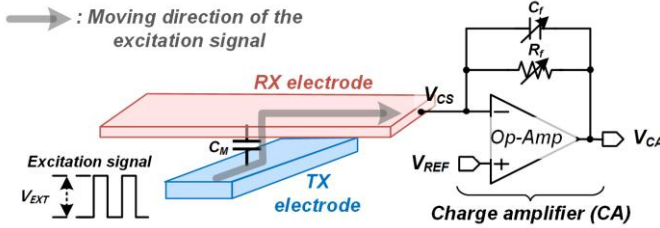


Fig. 4. Block diagram of the charge amplifier (CA).

operates as a LPF, the CA and CTS together have the electrical characteristic of a first-order BPF. However, because the cut-off frequency of the BPF varies according to the position of the sensor pixel, noises and signals with f_{EX_H} cannot be fully attenuated. To accurately filter out noises and signals with f_{EX_H} , the synchronized BPF implemented in the readout circuit is designed to have a mid-frequency synchronized with f_{EX} . The demodulator demodulates the output voltage of the BPF (V_{BPF}) to a DC signal and modulates the noises and signals with f_{EX_H} to high frequency spectra. The LPF is used to attenuate the modulated noises and the chopping ripple generated by the demodulator. Thus, the ACS method quickly detects external noises using the ACC and achieves a high SNR by filtering out external noises using the chopper stabilization method with synchronous BPF in the readout circuit.

IV. CIRCUIT IMPLEMENTATION OF ROIC

A. Charge Amplifier (CA)

Fig. 4 shows the block diagram of the CA, which consists of an operational amplifier (Op-Amp), a variable feedback capacitor (C_f), and a variable resistor (R_f). The excitation signal, which has the amplitude of V_{EXT} , is sent to each CA via a mutual capacitor having the value of C_M . Each CA then converts the V_{CS} to the V_{CA} , which is adjusted by C_f and given by

$$V_{CA} = V_{REF} - \frac{C_M}{C_f} \times V_{EXT}, \quad (3)$$

where V_{REF} is the reference voltage to bias the Op-Amp. To reduce the interference from 60 Hz noise, R_f is added to operate the CA as a high-pass filter. The cut-off frequency of the CA (f_{C_CA}) is defined as $1/(2\pi \times C_f \times R_f)$. In the CA, C_f and R_f are designed to have an f_{C_CA} less than f_{EX} , and thus attenuate external noises while transferring V_{CS} .

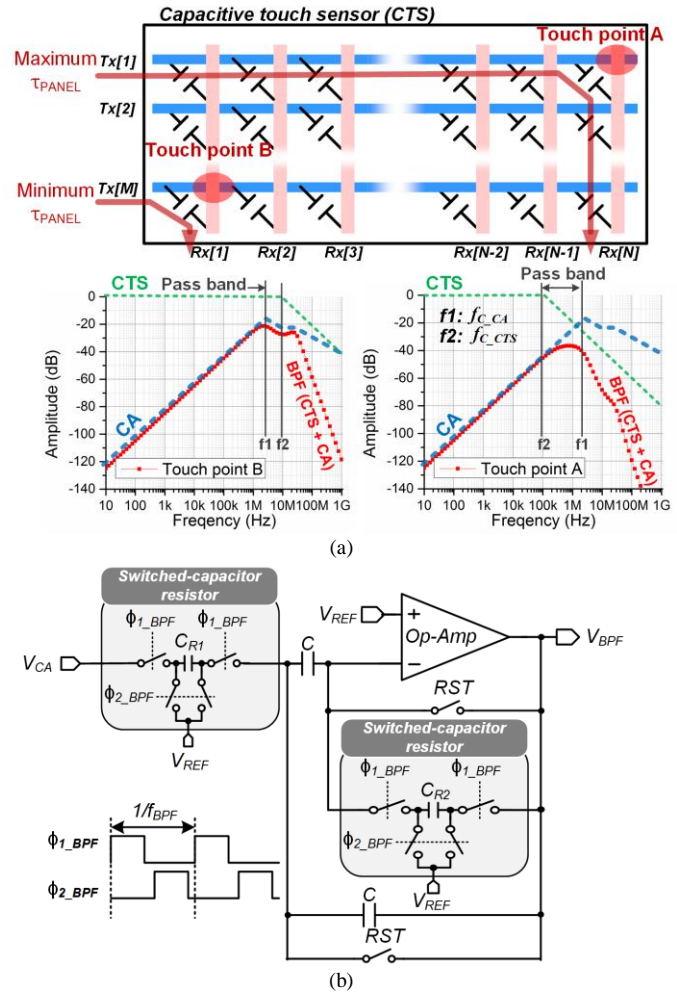


Fig. 5. (a) Simulated frequency response of the charge amplifier (CA) and capacitive touch sensor (CTS) and (b) schematic of a switched capacitor band-pass filter (SC-BPF) with multiple feedback topology (MFT).

B. Band-pass Filter (BPF)

The cut-off frequency of the CTS (f_{C_CTS}) is determined by the larger value of either (TX resistance \times TX stray capacitance) or (RX resistance \times RX stray capacitance) and is given by $f_{C_CTS}=1/(2\pi \times \tau_{CTS})$ where τ_{CTS} is the RC time constant of the CTS. Because τ_{CTS} varies according to the position of the touch point on the CTS, f_{C_CTS} also varies in this way.

Fig. 5(a) shows the simulated frequency responses of the CA and the CTS according to the positions of the touch point. When the CTS is touched at touch point A, f_{C_CTS} becomes smaller than the bandwidth of the CA because τ_{CTS} has its maximum value. Thus, the pass-band frequency range is determined by both the CA and the CTS. On the other hand, when the CTS is touched at touch point B, τ_{CTS} has its minimum value, and f_{C_CTS} increases. Thus, the pass-band frequency range is determined by CA only. Because τ_{CTS} varies according to the position of the touch point, external noises are not evenly attenuated. Therefore, a BPF is implemented in the readout circuit to effectively reduce external noises.

In addition, a switched-capacitor band-pass filter (SC-BPF) is adopted to accurately adjust the mid-frequency (f_m) [16]-[18]. Furthermore, a multiple feedback topology (MFT) is employed in the SC-BPF to have a constant gain at f_m regardless of

variation in f_m . Fig. 5(b) shows the schematic of the SC-BPF with MTF, which consists of an Op-Amp, two reset switches, two switched-capacitor resistors, and two capacitors. The mid-frequency (f_{m_SC}) and gain (G_{m_SC}) of the SC-BPF can be expressed as

$$f_{m_SC} = \frac{f_{BPF} \times \sqrt{(C_{R1} \times C_{R2})}}{(2 \times \pi \times C)}, \quad (4)$$

$$G_{m_SC} = \frac{C_{R1}}{(2 \times C_{R2})}, \quad (5)$$

respectively, where f_{BPF} is the frequency of the control signals for the SC-BPF (Φ_{1_BPF} and Φ_{2_BPF}). Because both f_{m_SC} and G_{m_SC} are determined by ratios of capacitances (C_{R1} , C_{R2} , and C), they are negligibly affected by process variation. Moreover, f_{m_SC} can be more accurately controlled by adjusting the capacitance ratio. The f_{BPF} is designed to be 10-times higher than f_{EX} to avoid aliasing. In addition, because f_{BPF} is synchronized to $10 \times f_{EX}$, f_{m_SC} is inherently adjusted to f_{EX} . Therefore, the BPF in the readout circuit can accurately reduce the remaining external noises.

C. Demodulator

Fig. 6 shows the schematic of the demodulator, which consists of a chopper amplifier with two chopper switch blocks, two coupling capacitors (C_1 and C_2), two resistors (R_1 and R_2), four reset switches, and two multiplexers. The output voltage of the demodulator (V_{DE}) is determined to be $(C_1/C_2) \times V_{BPF}$, and R_1 and R_2 are used to bias the nodes V_{INP} and V_{INN} , respectively. The ripple of V_{DE} is reduced by placing the chopping switch blocks at the low impedance nodes, which are the source nodes of transistors M_1 - M_2 and M_3 - M_4 in the chopper amplifier [19]-[20]. In addition, a compensation capacitor (C_{COMP}) between the drain node of transistors (M_2 and M_4) and the output node of the demodulator is implemented to reduce the bandwidth of the chopper amplifier, and thereby to further attenuate the ripple of V_{DE} .

D. Low-pass Filter (LPF)

The LPF is implemented as a buffer using a switched-capacitor LPF (SC-LPF) with Shallen-Key topology to achieve high gain control accuracy because its gain at low frequency is independent of process variations [17]-[18]. Fig. 7 shows the SC-LPF, which consists of an Op-Amp, two switched-capacitor resistors, and two capacitors (C_1 and C_2). The cut-off frequency of the SC-LPF (f_{C_SC}) can be expressed as

$$f_{C_SC} = \frac{C_{R1} \times f_{LPF}}{2\pi\sqrt{C_1 C_2}}, \quad (6)$$

where f_{LPF} is the frequency of the control signals (Φ_{1_LPF} and Φ_{2_LPF}) for the SC-LPF. Because the switched-capacitor resistors are used in the LPF, f_{C_SC} is determined by the ratio of capacitances (C_{R1} , C_1 , and C_2); thus, the variation in f_{C_SC} can be reduced compared with that of a conventional LPF. Moreover, because f_{C_SC} can be controlled by adjusting f_{LPF} , the ROIC can be easily operated at various frame rates.

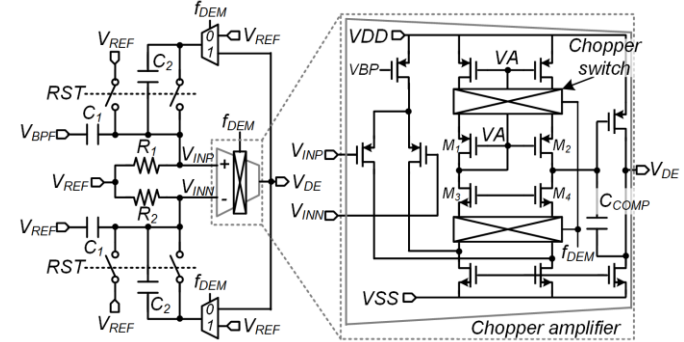


Fig. 6. Schematic of the demodulator with a chopper amplifier.

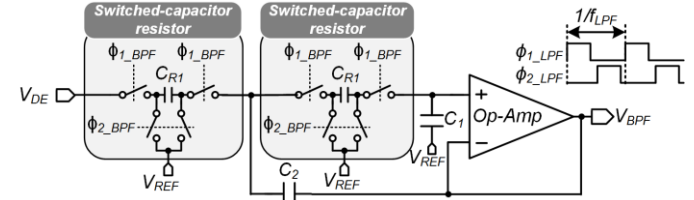


Fig. 7. Schematic of the switched capacitor low-pass filter (SC-LPF) with Shallen-Key topology.

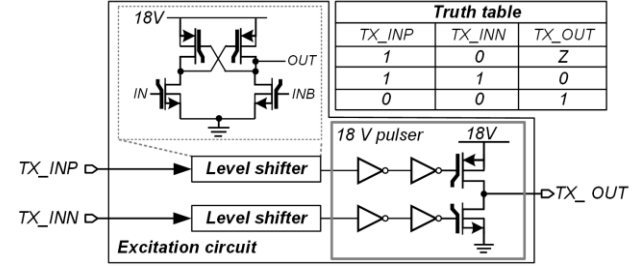


Fig. 8. Schematic of the excitation circuit.

E. Excitation circuit

Fig. 8 shows the excitation circuit, which consists of two level shifters and an 18 V pulser, by using the laterally double-diffused MOSFETs [21]. The two control signals (TX_INP and TX_INN), which originated from ACC, are induced into level shifters, respectively. According to the states of the TX_INP and TX_INN , the output voltage of 18 V pulser (TX_OUT) is decided to high impedance (Z), low (0 V), and high (18 V) as shown in the truth table in Fig. 8.

V. EXPERIMENTAL RESULTS

A. Measurement Setup

The proposed CTSS was implemented with a 46-inch CTS consisting of 120 RX and 70 TX electrodes. The CTS, which uses a metal mesh structure, is covered with a 4.0 mm thickness glass and mounted on the full-high definition liquid crystal display with a 4.0 mm air gap. Both the TX and RX electrodes are made of Ag with a metal width of 10.0 μ m and a sheet resistance of less than 7.0 Ω/\square .

The proposed ROIC was fabricated using a 0.35 μ m standard CMOS process technology with 18 V high-voltage devices. Fig. 9 shows a chip microphotograph of the ROIC, which occupies an area of 5,000 μ m \times 5,000 μ m. The fabricated chip includes 44-channel excitation and readout circuits, an interface and

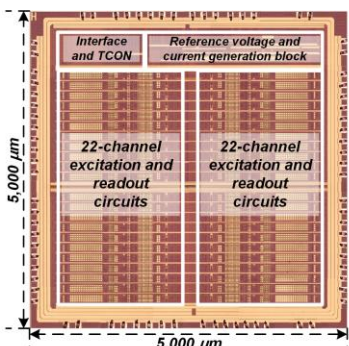


Fig. 9. Chip microphotograph of the ROIC.

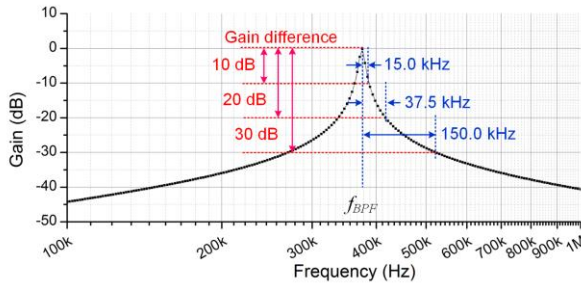


Fig. 10. Frequency response of the second-order BPF.

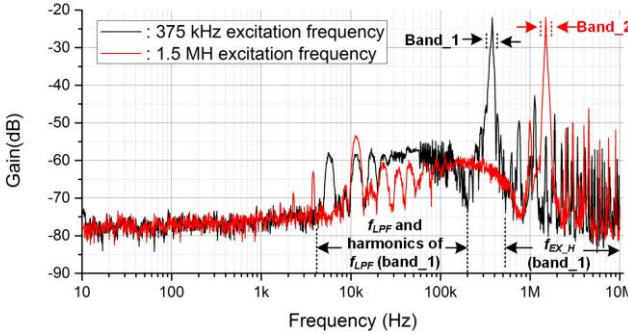


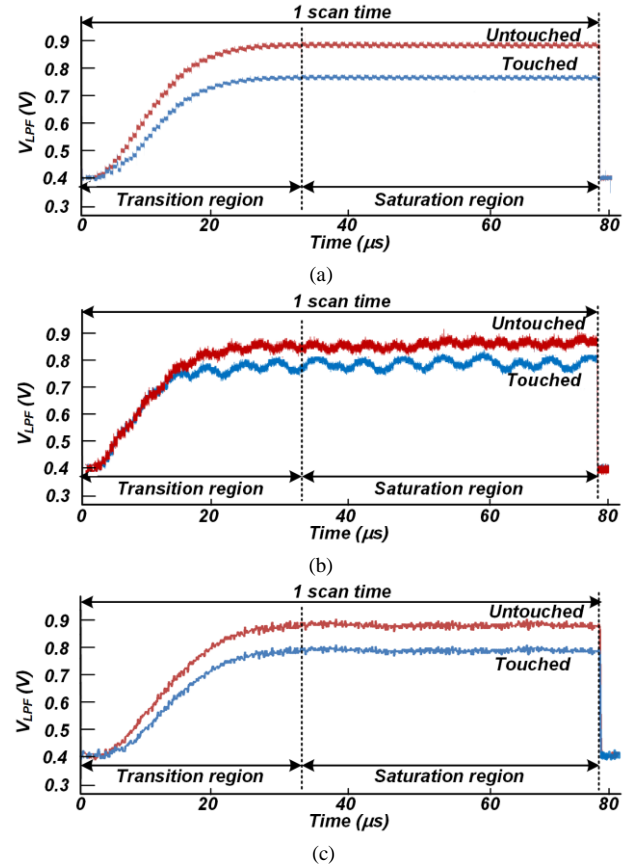
Fig. 11. Frequency response of the readout circuit.

timing controller (TCON), and reference voltage and current generation blocks. The ACC is implemented in the proposed ROIC by using a field programmable gate array (FPGA).

To determine the D_{NOISE_REF} and the f_{EX} values $f_{EX}(k+1)$, $f_{EX}(k+2)$, and $f_{EX}(k+3)$, the frequency response of the second-order BPF, which has a roll-off of $-40 [16], was measured as shown in Fig. 10. Because f_{EX} is located at the 10-times the upper frequency limit of the external noises, the amplitude of external noises is attenuated by 40 dB. Therefore, the D_{NOISE_REF} is set to have an SNR of over 40 dB in the ROIC. The values $f_{EX}(k+1)$, $f_{EX}(k+2)$, and $f_{EX}(k+3)$ are determined to improve the SNRs of the ROIC by 10, 20, and 30 dB by shifting f_{EX} by 15.0, 37.5, and 150.0 kHz, respectively. Therefore, 15.0, 37.5, and 150.0 kHz were assigned to $f_{EX}(k+1)$, $f_{EX}(k+2)$, and $f_{EX}(k+3)$, respectively, to measure the performance of the readout circuit.$

B. Measurement Results for ACS Method

Fig. 11 shows the frequency response of the readout circuit. When the readout circuit operates at f_{EX} of 375 kHz and 1.5

Fig. 12. Measurement results of the V_{LPF} in a scan time (a) without external noise, (b) without the ACS method (with external noise), and (c) with the ACS method (with external noise).

MHz, the measured pass-band frequencies of the touch signal are located at band_1 and band_2, respectively, while maintaining a maximum gain. These measurement results show that the gain difference of the readout circuit between signals at f_{EX} and other frequencies is distributed from 33.1 to 51.4 dB. The SNR [6] is defined by

$$SNR (dB) = 20 \times \log(S_{Touch} / N_{RMS}), \quad (7)$$

$$N_{RMS} = \sqrt{\frac{\sum_{n=0}^{99} \left\{ Touch\ data_{Touch}[n] - \left(\sum_{n=0}^{99} Touch\ data_{Touch}[n] \right) / 100 \right\}^2}{100}}, \quad (8)$$

where S_{Touch} is the average value of differences in 100 touch data at touched and untouched, and $Touch\ data_{Touch}$ is touch data at touched.

Fig. 12 shows the measurement results of V_{LPF} in a scan time, which is divided into transition and saturation regions. In the transition region, the LPF filters out V_{DE} and gradually increases V_{LPF} , of which the settling time depends on the cut-off frequency of the LPF. In the saturation region, the V_{LPF} becomes saturated at the end of one scan time and is then sampled by the SS-ADC. To verify the ACS method in the time domain, external noise with a sinewave of 375 kHz and 10 V peak-to-peak amplitude is directly induced into the CTS via 15-mm-diameter conductor. Fig. 12(a) shows the measured

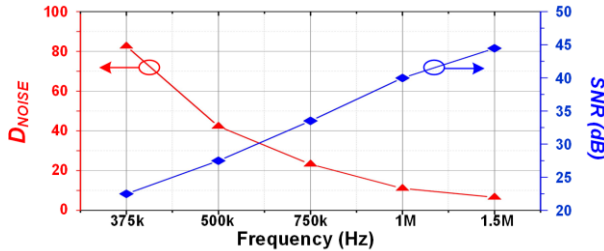


Fig. 13. D_{NOISE} and SNR versus excitation frequency under conditions of external noise (375 kHz, 10 V peak-to-peak sine wave).

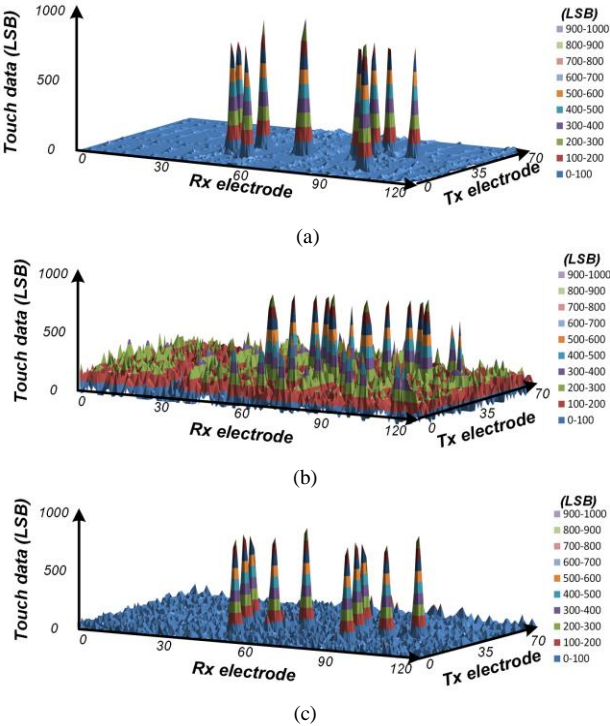


Fig. 14. 3D images of 10-point multi-touch: (a) without external noise, (b) without the ACS method (with external noise), and (c) with the ACS method (with external noise).

V_{LPF} without any induced external noise when the CTS is untouched and touched. Fig. 12(b) and (c) show the measured V_{LPF} with induced external noises, without and with the use of the ACS method, respectively. When the ACS method is not used, the V_{LPF} varies by a peak-to-peak voltage of 86.1 mV in the saturation region, when f_{EX} is near the frequency of the external noise. On the other hand, when the ACS method is used, V_{LPF} varies by a peak-to-peak voltage of 9.6 mV under the same external noise conditions, representing a reduction of 88.6 % compared with the peak-to-peak variation in V_{LPF} when the ACS method is not used.

Fig. 13 shows D_{NOISE} and SNR versus excitation frequency under conditions of external noise induced into the CTS. As f_{EX} increases, it moves farther from the frequency of external noise; thus, the external noise becomes gradually more attenuated, and thereby D_{NOISE} decreases from 104.0 to 9.1, which results in increasing the SNR from 22.5 to 44.5 dB. Thus, the ACS method effectively improves the SNR by 22.0 dB under the same external noise condition.

Fig. 14 shows 3D images of 10-point multi-touch using a

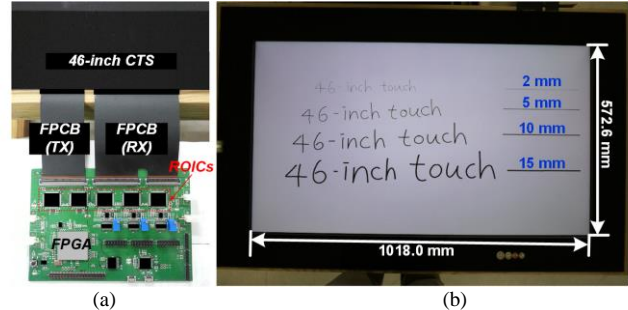


Fig. 15. Experimental demonstration of CTSS: (a) evaluation board system, (b) demonstration of 46-inch CTS using various conductor diameters; 2 mm (first sentence and line), 5 mm (second sentence and line), 10 mm (third sentence and line), and 15 mm (fourth sentence and line).

TABLE I
PERFORMANCE COMPARISON BETWEEN THE PROPOSED ROIC AND PREVIOUSLY REPORTED WORKS.

	This work	[9]	[10]	[12]
CMOS process (μm)	0.35	0.35	0.35	0.18
Size of CTS (inches)	46	10.1	23	70
Resolution of CTS	120×70	43×27	12×16	248×140
Frame rate (Hz)	120	120	175	120
SNR w/o noise (dB)	45.8	39.0	27.0	31.5
SNR w/ noise (dB)	44.5	N/A	N/A	N/A
Power consumption (mW)	180.5	18.7	76.0	1247.0
Power consumption / # of sensor pixels (μW)	21.5	16.1	395.8	36.0

46-inch CTS, which has 120 RX and 70 TX electrodes, under the above measurement condition of external noise (375 kHz, 10 V peak-to-peak sine wave). When no external noises are induced into the CTS, 10 multi-touch points in the 3D image are easily visible as shown in Fig. 14(a). Fig. 14(b) and (c) show the 3D images without and with the use of the ACS method, respectively, when external noises are induced into the CTS. Without the use of the ACS method, all touch data at untouched points are increased and additional glitches caused by external noises are observed near 10 multi-touch points, making it difficult to detect the actual touch points. On the other hand, with the use of the ACS method, all touch data at untouched points are decreased and additional glitches are disappeared, thereby the actual touch points can be easily detected.

Fig. 15 shows an experimental demonstration of the CTSS with a 46-inch CTS. In the evaluation board system, 5 ROICs and an FPGA are assembled together with a 46-inch CTS by means of flexible printed circuit boards (FPCBs) for TX and RX electrodes, as shown in Fig. 15(a). Various conductor diameters of 2, 5, 10, and 15 mm are used to demonstrate the touch resolution as shown in Fig. 15(b).

As summarized in Table I, the performance of the proposed ROIC is compared with that of the previously reported works [9]-[10], [12], showing that the proposed ROIC achieves the highest SNR. In addition, the measurement result shows that when the external noises are induced, the SNR with the use of the ACS method differs only 1.3 dB from that without any induced external noise. Thus, the ACS method effectively filters out external noises, thereby achieving high noise

immunity of the CTSS.

VI. CONCLUSIONS

In this paper, we propose an ROIC that employs an ACS method to filter out external noises quickly and adaptively. The proposed ROIC achieves high noise immunity against any external noises. The measured SNR of the proposed ROIC using 46-inch CTS is 45.8 dB at a reporting rate of 120 Hz, which is the highest SNR compared with that of the prior works. The SNR of the ROIC with the use of the ACS method is improved by 22.0 dB compared with that without the use of the ACS method. Therefore, the proposed ROIC, which adopts the ACS method, is appropriate for highly noise-immune CTSS.

REFERENCES

- [1] R.N. Aguilar and G.C.M. Meijer, "Fast interface electronics for a resistive touch screen," in *Proc. IEEE Sensors*, vol. 2, pp.1360–1363, 2002.
- [2] R. Adler and P. J. Desmares, "An economical touch panel using SAW absorption," *IEEE Trans. Ultrasonics, Ferroelectrics, and Frequency Control*, vol. 34, no 2, pp. 195–201, 1987.
- [3] S. H. Bae *et al.*, "Integrating multi-touch function with a large-sized LCD," *Soc. Inf. Display(SID) Symp. Digest*, pp. 178–181, 2008.
- [4] T. H. Hwang, W. H. Cui, I. K. Yang, and O. K. Kwon, "A Highly Area-Efficient Controller for Capacitive Touch Screen Panel Systems," *IEEE Trans. Consumer Electronics*, vol. 56, issue. 2, pp. 1115-1122, May, 2010.
- [5] B. Liu, K. S. Lee, and Y. M. Lee, "On-Chip Touch Sensor Readout Circuit Using Passive Sigma-Delta Modulator Capacitance-to-Digital Converter," *IEEE Sensors J.* vol. 15, no. 7, pp. 3893-3902, issue 7, 2015
- [6] S. Ko *et al.*, "Low Noise Capacitive Sensor for Multi-touch Mobile handset's applications," *IEEE Asian Solid-State Circuits Conf.*, Beijing, China, Nov. 8-10, 2010, pp. 1-4.
- [7] M.G.Stewart *et al.*, "Radiated Immunity Requirements for Equipment Operational during High Voltage Network Switching Operations", *IEE Proceeding on Generation, Transmission and Distribution*, Vol. 148, No. 6, pp 610-614, November 2001.
- [8] H. S. Kim and K. Y. Han, "High-SNR Capacitive Multi-Touch Sensing Technique for AMOLED Display Panels," *IEEE Sensors J.* vol. 16, no. 4, pp. 859-860, issue 15, 2016
- [9] J. H. Yang *et al.*, "A highly noise-immune touch controller using Filtered-Delta-Integration and a charge-interpolation technique for 10.1-inch capacitive touch-screen panels," *IEEE Int. Solid-State Circuits Conf. Digest Technical Papers*, San Francisco, CA, USA, Feb. 17-21, 2013, pp. 390-391.
- [10] J. S. Lee *et al.*, "An LCD-VCOM-Noise Resilient Mutual-Capacitive Touch-Sensor IC Chip with a Low-Voltage Driving Signal," *IEEE Sensors J.*, vol. 15, pp. 4595-4602, issue 8, 2015
- [11] I. S. Yang and O. K. Kwon, "A touch controller using differential sensing method for on-cell capacitive touch screen panel systems," *IEEE Trans. Consumer Electron.*, vol. 57, no. 3, pp. 1027–1032, Aug. 2011.
- [12] M. Hamaguchi, A. Nagao, and M. Miyamoto, "A 240Hz-reporting-rate 143×81 mutual-capacitance touch-sensing analog front-end IC with 37 dB SNR for 1mm-diameter stylus." *IEEE Int. Solid-State Circuits Conf. Digest Technical Papers*, San Francisco, CA, USA, Feb. 9-13, 2014, pp. 214-215.
- [13] K. D. Kim *et al.*, "A Capacitive Touchscreen Controller IC with Noise-based Hybrid Sensing Scheme," *SID Symposium Digest of Technical Papers*, Vancouver, British Columbia, Canada, May. 19-24, 2013, pp. 626-629.
- [14] C. H. Krah, S. P. Hotelling, S. E. O'Connor, and W. C. Westerman, "Detection of low noise frequencies for multiple frequency sensor panel stimulation," U.S. Patent 12/904,012. Nov. 13, 2010.
- [15] R. J. Baker, H. W. Li, and D. E. Boyce, *CMOS Circuit Design, Layout, and Simulation*. Piscataway, NJ: IEEE Press, 1998.
- [16] T. Kugelstadt, "Active filter design techniques," in *Op Amps for Everyone: Design Reference*, R. Mancini, Ed. Boston, MA: Newnes, pp. 271–281.
- [17] K. Martin, "Improved Circuits for the Realization of Switched Capacitor Filters" *IEEE Trans. Circuits and Systems*, pp. 237-244, April. 1980.
- [18] H. Irino, "Bandpass filter circuit," U.S. Patent 11/976,348. Dec. 24, 2007.
- [19] T. Denison *et al.*, "A 2 W 100 nV/rtHz chopper-stabilized instrumentation amplifier for chronic measurement of neural field potentials," *IEEE J. Solid-State Circuits*, vol. 42, no. 12, pp. 2934–2945, Dec. 2007
- [20] N. Verma *et al.*, "A micro-power EEG acquisition SoC with integrated feature extraction processor for a chronic seizure detection system," *IEEE J. Solid-State Circuits*, vol. 45, no. 4, pp. 804–816, Apr. 2010.
- [21] S.-J. Jung, J.-K. Song, and O.-K. Kwon, "Three-side buttable integrated ultrasound chip with a 16 16 reconfigurable transceiver and capacitive micromachined ultrasonic transducer array for 3-D ultrasound imaging systems," *IEEE Trans. Electron Devices*, vol. 60, no. 10, pp. 3562–3569, Oct. 2013.



Jae-Sung An (S'12) received a B.S. in Media Communications Engineering from Hanyang University in Seoul, Korea, in 2010. He is currently pursuing a Ph.D. Degree at Hanyang University, Seoul, Korea. His research interests include sensing methodologies and high-precision analog circuits for capacitive touch sensing systems.



Sung-Jin Jung (S'12) received a B.S. in Electronics Engineering from Hanyang University, Seoul, Korea, in 2009. He is currently working toward a Ph.D. at the same university. His research interests include high-voltage circuit design, high-precision analog circuits, and mixed-signal circuit designs for medical devices and systems.



Seong-Kwan Hong received a Ph.D. Degree in Electrical Engineering from the Georgia Institute of Technology, Atlanta, GA, USA, in 1994. He is currently a Research Professor at Hanyang University, Seoul, Korea.



Oh-Kyong Kwon (S'83–M'88) received a Ph.D. Degree in Electrical Engineering from Stanford University, Stanford, CA, USA, in 1988. He is currently a Professor in the Department of Electronic Engineering of Hanyang University, Seoul, Korea.